

Contents lists available at ScienceDirect

Spectrochimica Acta Part A: Molecular and Biomolecular Spectroscopy

journal homepage: www.journals.elsevier.com/spectrochimica-acta-part-a-molecular-and-biomolecular-spectroscopy





An optimized purification protocol for enzymatically synthesized S-adenosyl-L-methionine (SAM) for applications in solution state infrared spectroscopic studies

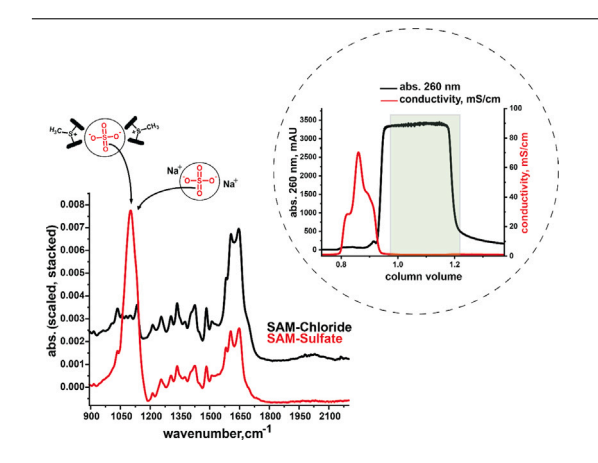
Isaiah Odeyemi ^a, Teri A. Douglas ^a, Nosakhare F. Igie ^a, James A. Hargrove ^a, Grace Hamilton ^a, Brianna B. Bradley ^a, Cathy Thai ^a, Brendan Le ^a, Maitri Unjia ^a, Dylan Wicherts ^a, Zackery Ferneyhough ^a, Anjali Pillai ^a, Shailendra Koirala ^a, Laurel M. Hagge ^a, Himanshu Polara ^a, Raymond C. Trievel ^b, Robert J. Fick ^a, Allison L. Stelling ^a,*

HIGHLIGHTS

Optimized method to remove interfering salts and counterions in SAM IR spectra.

- The first IR spectra of isotopically labeled methyl-d₃ SAM are presented.
- Isotope incorporation was used for band assignment.

GRAPHICAL ABSTRACT



ARTICLE INFO

Keywords: S-adenosyl-L-methionine L-methionine ATP Trans-methylation L-methionine adenosyl transferase Conformational dynamics Solution state infrared spectroscopy

ABSTRACT

S-adenosyl-L-methionine (SAM) is an abundant biomolecule used by methyltransferases to regulate a wide range of essential cellular processes such as gene expression, cell signaling, protein functions, and metabolism. Despite considerable effort, there remain many specificity challenges associated with designing small molecule inhibitors for methyltransferases, most of which exhibit off-target effects. Interestingly, NMR evidence suggests that SAM undergoes conformeric exchange between several states when free in solution. Infrared spectroscopy can detect different conformers of molecules if present in appreciable populations. When SAM is noncovalently bound within enzyme active sites, the nature and the number of different conformations of the molecule are likely to be altered from when it is free in solution. If there are unique structures or different numbers of conformers between different methyltransferase active sites, solution-state information may provide promising structural leads to increase inhibitor specificity for a particular methyltransferase. Toward this goal, frequencies measured in SAM's infrared spectra must be assigned to the motions of specific atoms via isotope incorporation at discrete positions. The incorporation of isotopes into SAM's structure can be accomplished via an established enzymatic synthesis using isotopically labeled precursors. However, published protocols produced an intense

E-mail address: stelling@utdallas.edu (A.L. Stelling).

^a The University of Texas at Dallas, 800 W. Campbell Rd., Richardson, 75080, TX, USA

b University of Michigan, 1150 W. Medical Center Dr., Ann Arbor, 48109, MI, USA

^{*} Corresponding author.

and highly variable IR signal which overlapped with many of the signals from SAM rendering comparison between isotopes challenging. We observed this intense absorption to be from co-purifying salts and the SAM counterion, producing a strong, broad signal at $1100~\rm cm^{-1}$. Here, we report a revised SAM purification protocol that mitigates the contaminating salts and present the first IR spectra of isotopically labeled CD³-SAM. These results provide a foundation for isotopic labeling experiments of SAM that will define which atoms participate in individual molecular vibrations, as a means to detect specific molecular conformations.

1. Introduction

S-adenosyl-L-methionine (SAM, also known as AdoMet) is an essential sulfonium molecule found in all living organisms [1–6] and plays an indispensable role in numerous biochemical processes [7–12]. SAM is synthesized by the enzyme methionine adenosyltransferase (MAT), also known as SAM synthetase, using the substrates L-methionine and adenosine-triphosphate (ATP) [13,14]. Its biosynthesis occurs in the cytoplasm of microbial cells or in the tissues of organisms, particularly the liver [15–18]. SAM is a vital biological molecule, as it is utilized in a wide array of biochemical reactions and is the second most commonly used substrate after (ATP) [19,20]. The molecular structure of SAM (Fig. 1) was first described by G. L. Cantoni, in 1952, who showed how the positively charged sulfur atom activates the carbon atoms adjacent to it, making them susceptible to nucleophilic attack [21,22].

SAM frequently serves as the biological methyl donating substrate for protein methyltransferases, an important class of drug targets, to regulate a wide range of essential cellular processes via methylation of different amino acids, such as lysines and arginines [7,23-31]. Dysregulation of several protein methyltransferases have been implicated in disease, particularly cancer, rendering them attractive targets for drug design [32-36]. However, designing small molecule inhibitors that target specific protein methyltransferases has remained challenging due to selectivity issues resulting in off-target effects in this large class of enzymes, and few compounds have made it to human trials and been approved by the FDA [28,37-42]. SAM is a conformationally flexible molecule and can adopt numerous conformations, as observed in crystal structures of different classes of SAM-dependent methyltransferases [43]. Additionally, NMR data indicates that SAM is multi-conformeric when free in solution and the molecule can adopt multiple energetically reasonable physical conformations when bound with methyltransferase active sites, underscoring its conformational dynamics [44-49]. Knowledge of the number of energetically permitted conformers and their spatial arrangements for the small molecule present in the solution is crucial to understanding any specific conformational poises that it can adopt within the active site of a given methyltransferase [15,50,51]. To gain insights into the number of available conformations present under a given set of conditions, solution-state structural studies are required to characterize SAM's molecular structure when free, and when bound to methyltransferases [52-57]. Although NMR spectroscopy has been widely used to investigate SAM dynamics, the timescales of NMR experiments may mask SAM conformations that are in rapid exchange. In contrast, vibrational spectroscopy offers exquisite sensitivity in detecting molecular conformations undergoing rapid exchange and is ideally suited for characterizing the conformational dynamics of SAM [52,56,58,59]. Structural knowledge gained from these studies can be leveraged in designing inhibitors that more effectively compete with the different molecular conformations that SAM adopts within a methyltransferase active site [60-63]. Here, we report a revised protocol for SAM's purification that eliminates excess salts that interfere with conformer detection using vibrational spectroscopy [64-68]. Utilizing the highly purified SAM obtained from this protocol, we present the first IR spectra of isotopically labeled CD3-SAM. This protocol will serve as the foundation for conducting comprehensive isotope studies, with the primary objective of accurately correlating the observed vibrational shifts in the molecule's IR spectrum to detect any conformational

Fig. 1. Enzymatic synthesis of SAM from L-methionine and ATP is catalyzed by MetK.

states that may exist when the molecule is free in solution. Finally, these studies will pave the way for detecting and characterizing which specific conformations SAM adopts when bound, and the non-covalent interactions it forms within the active sites of methyltransferases.

2. Experimental

2.1. Materials and methods

All chemicals used in this work were reagent grade. CD₃-L-Methionine was purchased from Aldrich. Adenosine-5'-triphosphate (ATP) and N-[Tris-(hydroxymethyl)methyl]-glycine (Tricine) were purchased from Sigma-Aldrich. Isopropyl-β-D-1-thiogalactopyranoside (IPTG) and Tris base were purchased from Fisher-Bioreagents. NaH₂PO₄, Na₂HPO₄, 2-Mercaptoethanol 99% (β ME), NH₄OH (28%–30% solution in water), and L-methionine (98%) were purchased from Acros Organics. Glacial acetic acid and hydrochloric acid were purchased from Fisher Chemicals. E. coli BL21 (DE3) chemically competent cells were purchased from Invitrogen. Lysozyme (egg-white) was purchased from Alfa Aesa. Nickel-nitrilotriacetic acid (Ni-NTA) resin (50% slurry in 20% ethanol) was purchased from G-Biosciences. CM Sepharose and CG50 weak cation-exchange resins were purchased from Sigma-Aldrich. Bio-Gel P-2 media (extra fine, $<45~\mu m$ wet) was purchased from Bio-Rad. QAE Sephadex A-25 was purchased from Cytiva. The plasmid which encodes S-adenosyl-methionine synthetase (MetK) was donated by Dr. Dewey McCafferty at Duke University. High-purity TraceMetal Grade nitric acid, H2O, and ICP-MS metal standards were purchased from Sigma-Aldrich.

2.2. Expression and purification of SAM synthetase (MetK or MetX)

The enzymatic synthesis of S-adenosyl-L-methionine (AdoMet) was catalyzed by *E. coli* MetK using L-methionine and ATP [21,65,69]. Incubation of cell media for protein expression was done using the incu-shaker from INFORS. Mechanical disruption of the E. coli cell wall was performed with a Qsonica sonicator [70]. The soluble protein was separated from cell debris using a Sorvall Lynx 6000 centrifuge from Thermo-scientific. MetK was overexpressed in E. coli and purified as previously published [69,71] and the SDS PAGE gel image of purified MetK is shown in **Supplementary Figure S1**. The MetK enzyme migrates at 43 kDa, which is consistent with the sequence published by George D. Markham [69]. The concentration of enzyme and SAM were routinely monitored, during and after production, using a Nanodrop One-c ultraviolet (UV)-visible spectrometer from Thermo-Scientific [72]. Detailed procedure for MetK expression and purification is provided in the Supplementary Data section 1.0.

2.3. SAM synthesis and purification

A typical 50 mL reaction consisted of the following reagents: 200 mM Tricine/HCl pH 8.7, 50 mM KCl, 30 mM MgCl₂, 8% v/v β ME, 15 mM ATP, 10 mM L-Methionine, and 75 mg of MetK. The reaction was placed on a shaker (95 rpm) at room temperature. SAM production was monitored using HPLC analysis at time points from 5 min to 240 min. Optimal SAM production with minimal SAH formation was observed at about 2 h 30 min, but for higher SAM yield the reaction was extended to about 3 h 30 min. Once the reaction was completed, the mixture was spun at 4000 xg for 10 min to remove the precipitated enzyme. The supernatant was decanted and filtered through a $0.8~\mu m$ syringe filter. A 10 mL CG50 ion-exchange column was equilibrated with 15 column volumes (CV) of 1.0 M ammonium acetate buffer (pH 5.0), followed by 10 CV of ultrapure water. The filtrate was then loaded onto the column using the sample pump, followed by washing with 30 CV of water to remove the nonbinding components of the reaction mixture. SAM was eluted with a 20 CV linear gradient of water to 100 mM hydrochloric acid followed by 10 CV of 100 mM hydrochloric acid. The purity of the fractions was determined by HPLC, and pure fractions were pooled and neutralized by titrating with QAE-carbonate slurry in water to pH 6.5. The neutralized solution was filtered through a 0.8 um sterile syringe filter to remove the QAE Sephadex resin. The filtrate was then concentrated by rotary evaporation and loaded on a 25 mL Biogel-P2 size-exclusion column which was equilibrated with 10 mM HCl or water. After sample injection from a 250 µL sample loop, 2.5 CV of 10 mM HCl or ultrapure water was used to elute SAM, followed by a column wash utilizing 2.5 CV of ultrapure water if HCl was used. Using 10 mM HCl increases the ionic strength of the mobile phase and gives better peak resolution, with pooled fractions neutralized with QAE carbonate. Fractions were analyzed using the HPLC method as described in Section 2.4.2 to determine the purity of the fractions. Fractions with pure SAM were pooled if they had a conductivity <3 mS/cm and concentrated using a rotary evaporator. Fig. 2 shows the schematic representation of the enzymatic synthesis and purification SAM. Ion-exchange chromatography and size-exclusion chromatography were conducted at 4 °C using medium-pressure Next-Generation Chromatography (NGC) from Bio-Rad laboratories [73].

2.4. Analytical methods and instruments

2.4.1. Preparation of QAE carbonate slurry

QAE Sephadex resin was hydrated in 1M NaCl and kept at room temperature overnight. 80 mL of hydrated QAE chloride was transferred into a 100 mL column (to account for swelling in the water wash) and equilibrated with 8-column volumes of 800 mM sodium carbonate solution, followed by washing with 20-column volumes of water. QAE carbonate was stored at room temperature.

2.4.2. HPLC analysis

High-performance liquid chromatography (HPLC) was performed using a Vanquish system equipped with a multi-wavelength UV detection from Thermo-Scientific. The HPLC is equipped with an auto sampler, expediting the analysis of multiple samples. HPLC analyses were performed with an HILIC XBridge Amide column (4.6 mm \times 150 mm, 3.5 μm), using acetonitrile and sodium citrate buffer (10 mM, pH 3.0 with 25 mM NaCl). The column compartment temperature (40 °C), pump (1.00 mL/min), and the system were allowed to stabilize for about 20 min while the baseline is monitored. The sample was run with a 4-minute gradient of 20% to 50% citrate buffer, followed by 4 min of 50:50%. The column was then re-equilibrated to 80:20% acetonitrile:citrate buffer for 7 min before the next sample. 5'-methyl-thioadenosine (MTA), adenosine, S-adenosyl-L-homocysteine (SAH), and SAM chloride eluted at 2.1, 3.1, 5.3, and 5.9 min respectively. HPLC data processing was performed using Chromeleon software.

2.4.3. IR analysis

The IR spectra were measured using a PerkinElmer FTIR spectrometer Spectrum 3, equipped with a Pike Technologies MIRacle Universal Attenuated Total Reflectance (ATR). IR measurements were taken at room temperature with 128 scans, 4 cm $^{-1}$ resolution, using ultrapure water as the background. The background spectrum was subtracted from the sample spectrum by the auto background-removal function on the IR spectrometer. 6 μL of ultrapure water was first run as background, followed by 6 μL of the sample. To prevent sample evaporation, a 25 μL Teflon cap from PIKE technology was used to cover samples during analysis. IR spectral datawere processed using PerkinElmer Spectrum software. Before normalization, a multipoint baseline was added using the interactive baselining function. After baseline and normalization of the IR spectra, the difference function was used to perform spectra subtraction to identify the differences between the spectra.

2.4.4. NMR analysis

Nuclear magnetic resonance (NMR) experiments were conducted using a Bruker Avance III 600-MHz instrument. The sample was prepared for analysis by several rounds of lyophilization and resuspension in $\rm D_2O$. The acquired data were analyzed using Topspin software from Bruker.

2.4.5. Mass spectroscopic analysis

Liquid chromatography-mass spectroscopy (LC-MS) was conducted using an Agilent 1100 HPLC with a C-18 column for separation and an AB Sciex 4000 QTRAP system for mass detection. The sample was prepared in a 1:1 acetonitrile:water solution and run on LC for 30 min with gradient elution from 10%–90% acetonitrile in $\rm H_2O$ (both 0.1% TFA).

ICP-MS was used to determine the amount of sodium, magnesium, potassium, and lithium ions in SAM samples prepared using the existing and the optimized methods. While sodium, magnesium, and potassium ions are possible contaminants that may be found in SAM through its synthesis and purification, a known concentration of $\rm Li_2SO_4$ was used as an internal standard to ensure comparable sample concentration. ICP-MS samples (83 mM SAM and 50 mM $\rm Li_2SO_4$) were prepared in 100% HCl at room temperature. Samples were subsequently diluted (1 $\rm \mu L:4~mL)$ with 3% HNO3, and run on an Agilent 7900 ICP mass spectrometer (Agilent Technologies) connected to a CETAC ASX-500 auto-sampler for sample injection. Control experiments were conducted in 3% HNO3 for background correction.

3. Results and discussion

The major challenge faced with the determination of the IR spectrum of aqueous SAM is the presence of a strong signal from the polyatomic counterion, which produces a strong absorption at 1100 cm⁻¹. This signal is likely due to the S=O stretching of a sulfate ion that originated from the sulfuric acid which was used to elute SAM from the ion exchange column in the existing protocol and co-purified with SAM as a counterion and as Na₂SO₄ salt [71,74,75]. This strong signal hinders the detection of the weaker signals from SAM's ground state vibrational transitions in a spectral region where C-H vibrations are expected to be observed specifically transitions from bending motions of the C-H bonds Fig. 3. Also, since it is difficult to determine the specific concentration of salt produced alongside SAM during purification, the subtraction performed to remove the IR signal of liquid water by using buffer as a "blank" during the background scans resulted in batch-to-batch inconsistencies, resulting in challenges in obtaining replicate spectra. Therefore, we sought to modify the conditions of original purification to eliminate the strong sulfate signal that overlaps with several IR signals in SAM that are important for confirmation of isotope incorporation. For example, the C-H bending modes that are expected to be impacted by deuteration at the reactive methyl group

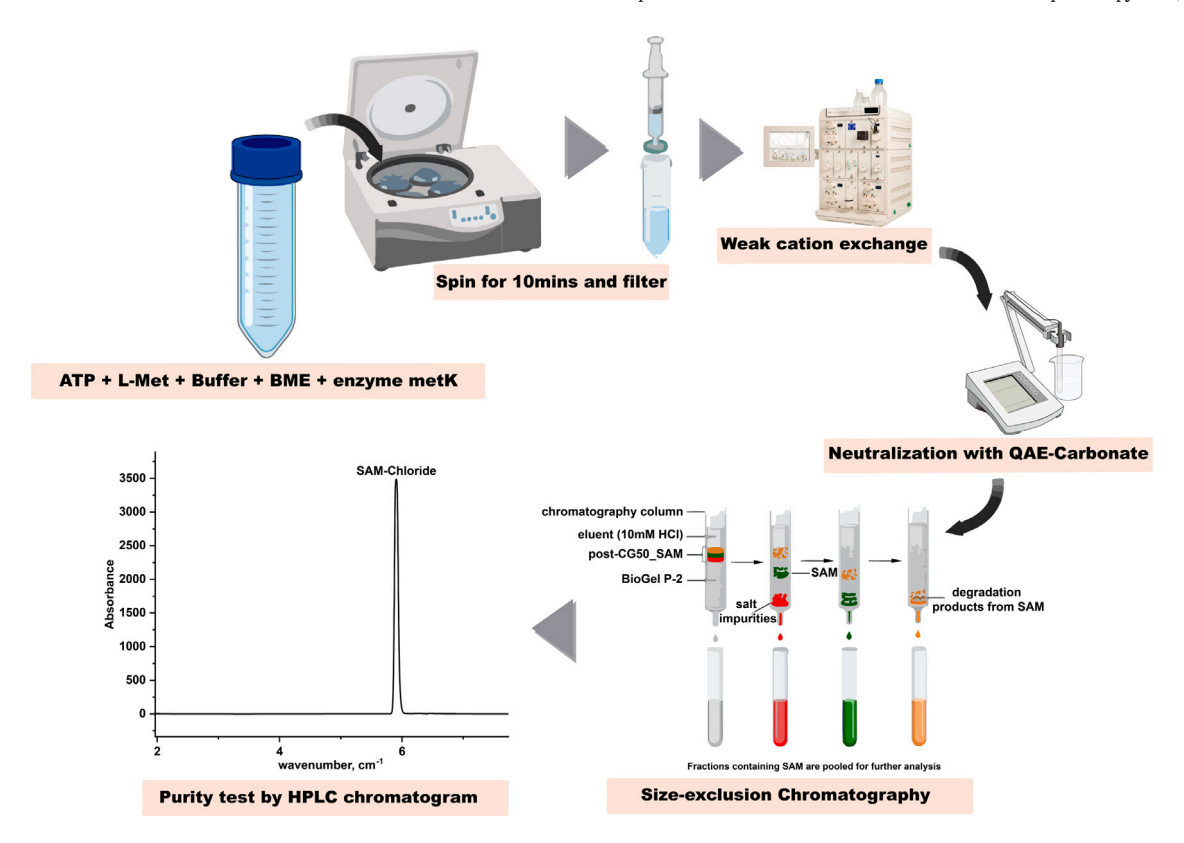


Fig. 2. Flowchart shows the optimized method for the synthesis and purification of SAM for infrared spectroscopic studies.

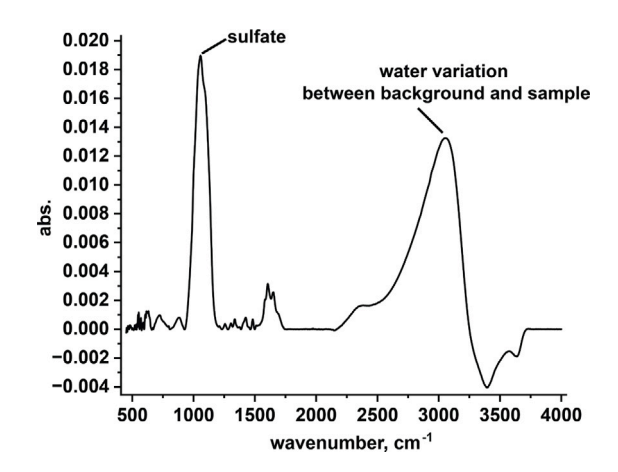


Fig. 3. IR spectrum of SAM shows the intense sulfate peak at $1100~\rm cm^{-1}$ that overlaps with the SAM vibrational signals and the poor background subtraction of the water "blank" due to high salt concentration ($3000~\rm cm^{-1}$). The absorption of the salt peak is 6-fold higher than the SAM's carbonyl signal and varies batch-to-batch.

cannot be observed in Fig. 3, due to the much more intense signal from the sulfates. The SAM enzymatic synthesis comprises two major steps: SAM production from an $S_{\rm N}2$ reaction between the methionine and adenosine moiety of ATP, followed by the second step which involves the hydrolysis of triphosphate to form pyrophosphate and orthophosphate, which happens before SAM is released from the enzyme([76] (Fig. 1: SAM reaction).

The existing protocol was altered in the following ways. The reaction buffer for the SAM reaction was changed to tricine, compared to the previous protocol in which Tris was used. This alteration was made because Tris can form a cationic species that binds alongside SAM to the weak cation exchange column at neutral pH. On the other hand, Tricine forms a zwitterion at physiological pH. Since both Tris

and Tricine have similar pKa values, Tricine is a better buffer option due to its zwitterionic property [77,78]. The concentration and pH of the reaction buffer were also changed to 200 mM pH 8.7 compared to 100 mM pH 8.0, used in the previous methods [67,79]. This alteration was introduced because as ATP is converted to SAM, acid is produced from the hydrolysis of the phosphoanhydride bond, lowering the pH of the reaction mixture [80-82]. MetK has an isoelectric point (pI) of 5.38 and becomes less soluble as the reaction pH approaches this value. Thus, both the concentration and the pH of the buffer were increased to enhance enzyme stability. The enzymatic synthesis was allowed to progress for 3 h and 30 min at room temperature. The SAM produced was purified, first with weak-cation exchange which removes the anions and neutral impurities such as 5'-methyl-thioadenosine (MTA), S-adenosyl-homocysteine (SAH), adenosine, and ATP. SAM and the cationic impurities in the reaction bind to the column and were eluted with a hydrochloric acid gradient (Fig. 4A). The weak cation exchange resin CM-52, a cellulose-based resin that was utilized in previous protocols [83] is no longer commercially available. CM-52 was replaced with CM-Sepharose, then with CG50, a methacrylic-based resin with a carboxylic functional group. CG50 was used in this study because it afforded a higher yield when compared with CM-Sepharose. SAM was eluted from the CG50 using 100 mM HCl in place of sulfuric acid used in the previous protocols. Conductivity increases across the linear gradient with increasing HCl which protonates the carboxylate groups on the CG50 column, resulting in the elution of SAM (Fig. 4A). As noted earlier, the IR spectra of SAM and the sulfate ion overlap each other, making detection of the SAM signals difficult in the presence of the strong sulfate signal. This problem was resolved by replacing the polyatomic sulfate counterion with the monatomic chloride counterion. In addition, the equilibration buffer was switched from sodium acetate, which was used in the previous protocols, to ammonium acetate for equilibration of the cation exchange column, with the goal of eliminating the resulting ammonium chloride by lyophilization. However, the ammonium chloride salt was not adequately removed due to its low vapor pressure of ammonium chloride at room temperature, and

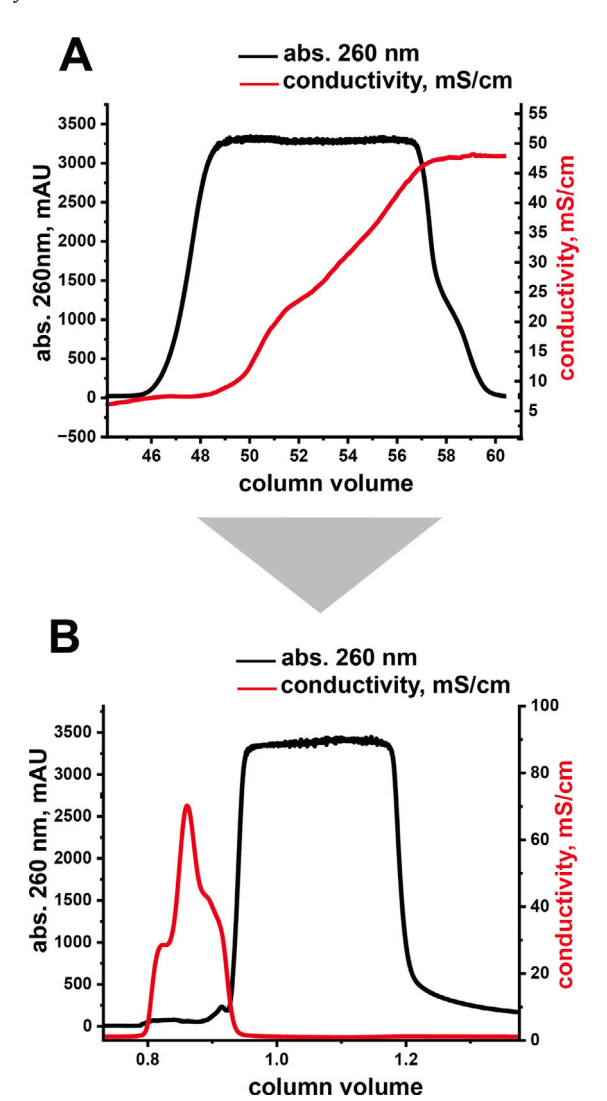


Fig. 4. (A) The CG50 weak cation exchange column was equilibrated with 1M ammonium acetate (pH 5.0), followed by linear gradient elution with 100 mM HCl. The black trace is the absorbance at 260 nm and the red trace shows conductivity as it increases across the plot. (B) Desalting of SAM using the Biogel-P2 column. SAM is observed to have some affinity with the column as salt elutes earlier and SAM elutes after one column volume.

heating the sample would lead to SAM degradation [66,84,85]. The ammonium chloride was observed to separate better from SAM than sodium chloride salt, allowing us to remove excess salt from SAM using the Biogel-P2 size exclusion chromatography step (Fig. 4B). SAM elutes the ion-exchange column at a pH value of 1.5. To study SAM at a neutral pH, the previously established methods used QAEhydroxide to neutralize the pooled fractions [83]. QAE Sephadex A-25 is a strong anion exchange resin that is sold as QAE-chloride and can be readily exchanged to a preferred counterion by washing with a high-concentration solution of the ion. QAE-hydroxide was prepared by washing QAE-chloride with sodium hydroxide. However, zero conductivity was not attained during the subsequent water wash in the preparation of QAE-hydroxide resin, indicating that there was residual sodium hydroxide within the resin. To circumvent this issue, we prepared QAE-carbonate resin by washing QAE-chloride with 800 mM sodium carbonate. Zero conductivity was attained upon washing with ultra-pure water suggesting a lack of contaminating sodium species. QAE-carbonate was used to neutralize SAM to a pH value of 6.5 and any ammonium carbonate formed during the neutralization decomposed in the vacuum during concentration using a rotatory evaporator or

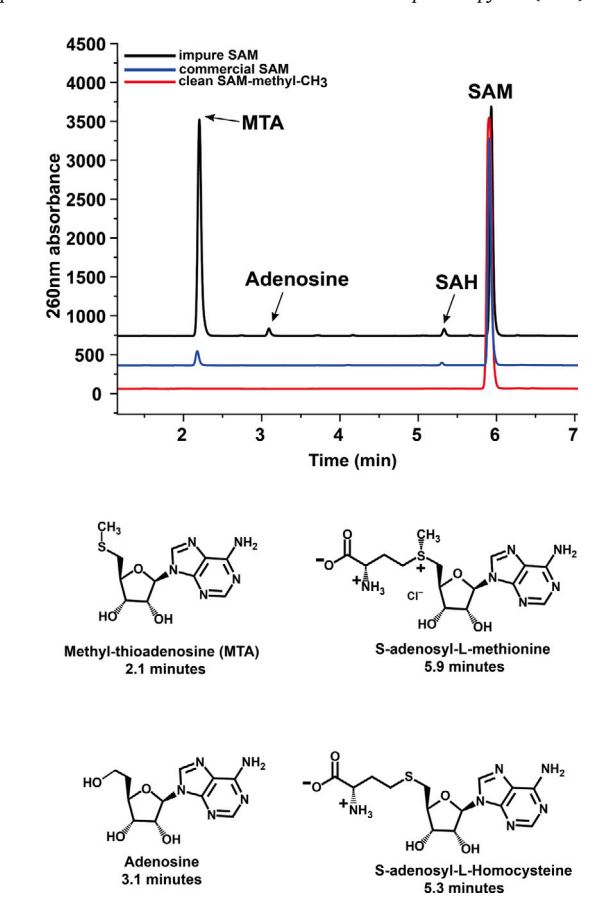


Fig. 5. The black trace was obtained from impure fractions of SAM that were deliberately taken for HPLC analysis during SAM purification. The fraction was found to contain impurities such as Adenosine, SAH, and MTA. The absorbance trace shown in blue was the commercial SAM and was found to contain MTA and SAH as impurities. The absorbance trace shown in red was the clean SAM synthesized and purified in our lab which contains none of the impurities found in both the impure and the commercial SAM

was separated in the next chromatography step. The next step involves desalting the SAM using Biogel-P2, a size exclusion resin, and eluting with 10 mM HCl or ultrapure water. Desalting was achieved by pooling fractions with the lowest to no conductivity (less than 3.0 mS/cm). Fresh Biogel-P2 resin was used for each purification to prevent transferring impurities to subsequent purifications. We observed that Biogel-P2 appears to have an intrinsic affinity for SAM and contaminants at low ionic strength, eluting past one column volume Fig. 4B. A chromatography system equipped with UV and conductivity detectors allowed us to assess SAM concentration and ionic strength when pooling fractions. This detection minimizes ionic contamination after the final column. Table S1 shows a summary of all the changes made to the previous protocol to obtain SAM adequate for IR studies.

3.1. HPLC

HPLC analysis was conducted to verify the purity of the SAM fractions after each column before pooling them. Fractions containing SAM from the first purification step were analyzed by HPLC as described earlier in Section 2.4.2 to confirm the absence of adenine-containing impurities. Fig. 5 shows the 260 nm absorbance trace of impure, commercial, and pure SAM.

3.2. Proton NMR

Proton NMR analysis was performed as discussed in Section 2.4.4. As expected, the ¹H-NMR did not show any difference between SAM

Table 1
ICP-MS values in parts per billion for the optimized and previous method, samples run in duplicate. The post BioGel sample for the previous method is representative of pooling by UV absorbance at 260 nm. Raw data is in Supplemental Table S2.

Sample	Lithium		Sodium		Magnesium		Potassium	
	mean	std. dev.	mean	std. dev.	mean	std. dev.	mean	std. dev.
50 mM lithium control	141.45	0.47	18.061	0.031	1.095	0.013	38.79	0.13
Opt. post CG50	139.6	2.3	40.37	0.73	574.9	8.8	262.3	3.5
Opt. BioGel fr 12-15	139.7	1.7	40.053	0.042	1206	11	109.42	0.014
Opt. BioGel fr 16	159.9	1.1	10.741	0.033	273.7	1.1	40.20	0.14
Opt. BioGel fr 17–23	157.336	0.047	18.296	0.029	39.54	0.35	39.92	0.79
Prev. post CG50	160.81	0.93	2842	20.	1963	26	558.9	3.1
Prev. post BioGel	154.68	0.33	1957	21	672.0	9.1	334.4	4.9
Prev. BioGel fr 7–12	147.6	2.1	3582	58	2388	41	710.	12
Prev. BioGel fr 13-16	154.9	1.6	157.7	1.7	202.9	1.5	56.04	0.61

with low or high conductivity. Supplemental Figure S11 shows the $^1\mathrm{H-NMR}$ spectrum of pure $\mathrm{CH_3-SAM}$ (low conductivity). The pure $\mathrm{CH_3-SAM}$ was overlayed with high conductivity-SAM (high conductivity fractions of SAM) to ascertain whether there are any differences in their spectra. No significant difference was observed. SAM has two chiral centers which result in four possible stereoisomers. The sulfonium chiral center can racemize to form (S)- and (R)-epimers, which are optically stable and can be separated. However, only the (S)-epimer is the only biologically active form of SAM. The (S)-epimer is observed as a singlet peak, 3H of the methyl-CH₃ at 2.92 ppm, and the (R)-epimer at 2.88 ppm (Sup. Fig. S11).

Matos and Wong studied the stability and stabilization of SAM and reported the major factors that affect the stability and epimerization of the (S)-epimer to (R)-epimer of SAM are the pH, temperature, and sulfonium counterion [66]. Mark L. et al. studied the stereochemistry of SAM in D_2O using NMR by measuring the coupling constants between the protons on the chiral centers [86]. Finally, there have also been several NMR studies of the conformational dynamics of SAM in solution [49].

3.3. ESI-MS

ESI-MS analysis illustrates the mass to charge (m/z) ratio of non-labeled SAM-chloride of 399.04 (m/z M+ calculated for $\rm C_{15}H_{23}N_6O_2S^+$ is 399.15), similar to commercial SAM which has an m/z value of 399.2 (Fig. 6A, B). As expected, fractions with high conductivity also exhibit a similar m/z ratio of 399.36 (Fig. 6D). Isotopically labeled CD $_3$ -SAM-chloride displays an m/z value of 402.32 ($\rm C_{15}D_3H_{20}N_6O_2S^+$ is 402.16) (Fig. 6C). A column background was obtained by blank injection into the mass spectrometer Supplementary Figure S2.

3.4. ICP-MS

Table 1 shows the differences in key ions between the two SAM purification protocols. Using ammonium for equilibration of the CG50 column eliminates the sodium that would be bound to the column initially, and largely reduces the sodium in the purification. Magnesium and potassium will still be present at similar levels in the reaction as their concentrations were unchanged, and they appear to persist through both purifications, although at a slightly reduced level in the optimized purification. The major point of difference seen between the two methods is that fractionation by conductivity after the BioGelP2 column is more effective at yielding a sample with reduced ionic content (Opt. BioGel fr 17–23 vs. Prev. BioGel fr 13–16). The ICP-MS results do not show ammonium content, but excess ammonium would be visible by the characteristic peak at 1450 cm⁻¹ in the IR spectrum.

3.5. IR analysis

The IR spectra of SAM obtained using the previous purification protocol indicate the presence of excess salt in the product after the final purification step, resulting in a strong IR signal at $\sim 1100~\rm cm^{-1}$

that likely arises from the S=O stretching of the sulfate counterion and the excess sodium sulfate salt [74,75]. Previous protocols elute SAM with sulfuric acid, contributing to the presence of the sulfate ions in the purified SAM [87,88]. Fig. 7A shows the IR spectrum of the final mixture containing both SAM and the sulfate counterion. Evidence for the signal being due to molecular vibrations from the sulfate ion and not SAM is evident as the interfering signal exhibits a large shift in positions (from ${\sim}1100~\text{cm}^{-1}$ to ${\sim}1450~\text{cm}^{-1}$) when a different salt is present in the purification. Fractions with high conductivity from the Biogel P2 column possess an intense ammonium ion peak at 1450 cm⁻¹ region [89-91] (Fig. 7B). However, fractions containing low to no conductivity (<3.0 mS/cm) lack salt impurities and the ammonium ion peak as seen in the black trace (Fig. 7B). Replicate, batch-to-batch (separate purifications) spectra of SAM-chloride were taken, with their mean and standard deviation plot shown in Fig. 8. Having confirmed the reproducibility of our method with the light isotopes, CD3-SAM was enzymatically synthesized utilizing a commercially available isotopically labeled precursor, CD3-L-Methionine, and our optimized SAM purification scheme. The synthesis of CD₃-SAM was confirmed using IR spectroscopy to compare the C-H and C-D stretching regions between the light and heavy isotopes of SAM. Fig. 8A below represents the mean and standard deviation plot of two-batch replicates of CD₃-SAM, with the bold line denoting the mean and the gray-shaded region illustrating the standard deviation. Depicted in green is the noise line obtained from the CD₃-SAM spectra. Fig. 8B depicts the CH₃-SAM IR spectrum and the noise line (shown in red) obtained by averaging the difference between the spectrum of the same batch of purified SAM. As expected, perturbation in the 1100 cm⁻¹ region of the CD₃-SAM spectrum is due to C-H stretching. The observed perturbations indicate the successful incorporation of the deuterated isotope. These expected perturbations are seen in the difference spectrum taken between CH3-SAM and CD₃-SAM Fig. 9.

4. Conclusion

The assignment of the infrared (IR) signals from S-adenosylmethionine in solution to the motions of specific atoms in its molecular structure via isotope labeling experiments has been complicated by the presence of a strong signal from the counterion resulting from its purification and salt that co-purify with SAM after its synthesis. These ions produce an IR signal far stronger than SAM, masking its signals and rendering detection of key spectral regions challenging [71]. The optimized purification method described here effectively removes these ionic hindrances to the detection of SAM's IR signals, which are otherwise undetectable via other methods such as NMR, mass spectroscopy, HPLC, and electron paramagnetic spectroscopy (EPR) [67,71,86,92] and enables the acquisition of high-quality IR spectra of naturally abundant and isotopically labeled SAM in the solution state. The spectral signal exhibits excellent signal-to-noise ratios, allowing for precise spectral analysis and assignment of transitions from specific functional group normal modes to the observed signals in SAM's IR spectrum. Our results pave the way for assigning observed frequencies

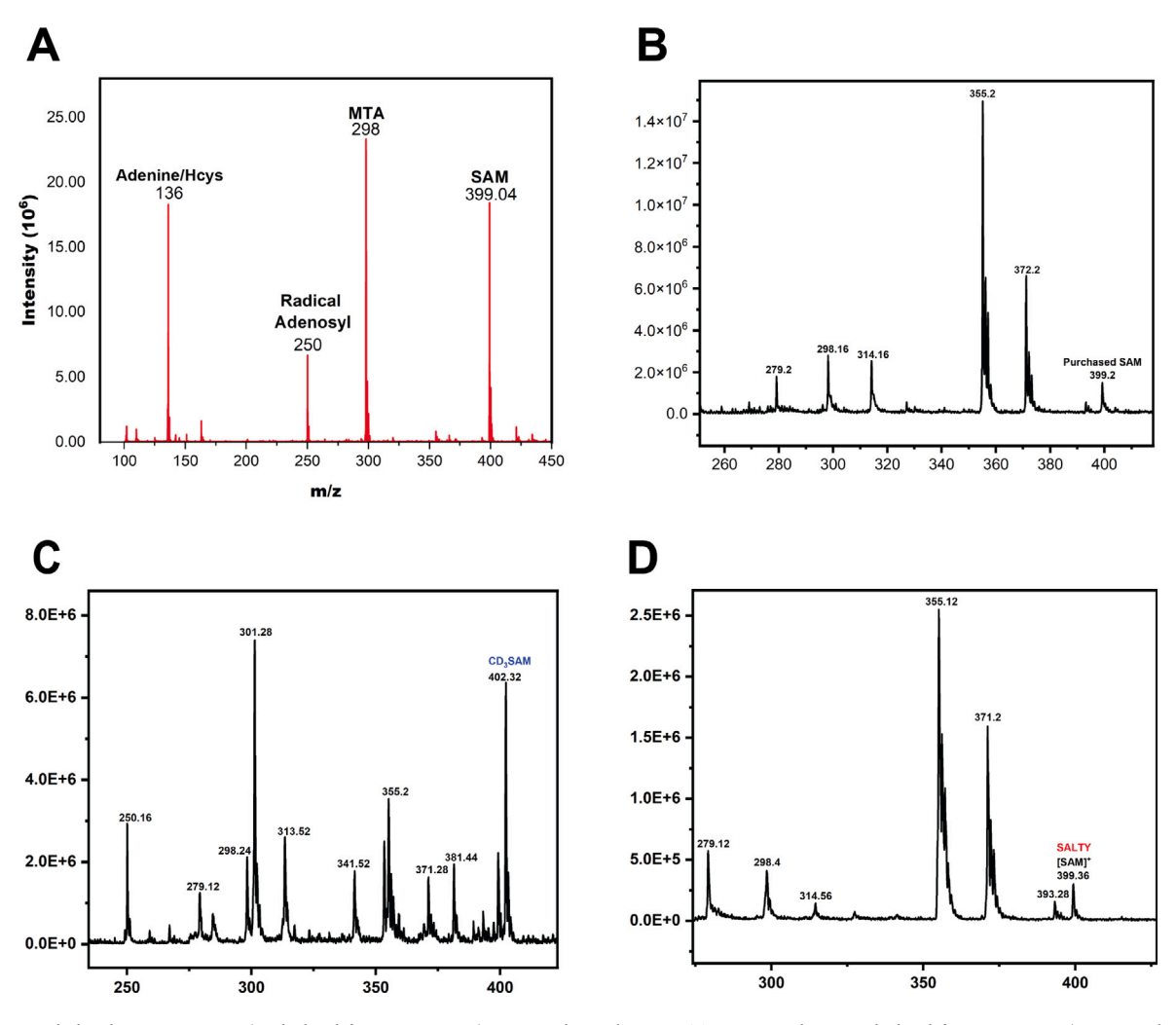


Fig. 6. (A) Natural abundance SAM m/z M $^+$ calculated for $C_{15}H_{23}N_6O_2S^+$ 399.15; observed 399.04 (B) Commercial SAM, calculated for $C_{15}H_{23}N_6O_2S^+$ 399.15; observed 399.2 (C) CD $_3$ -SAM: calculated for $C_{15}D_3H_{20}N_6O_2S^+$ 402.16; found 402.32 (D) High conductivity-SAM, calculated for $C_{15}H_{23}N_6O_2S^+$ 399.15; observed 399.36.

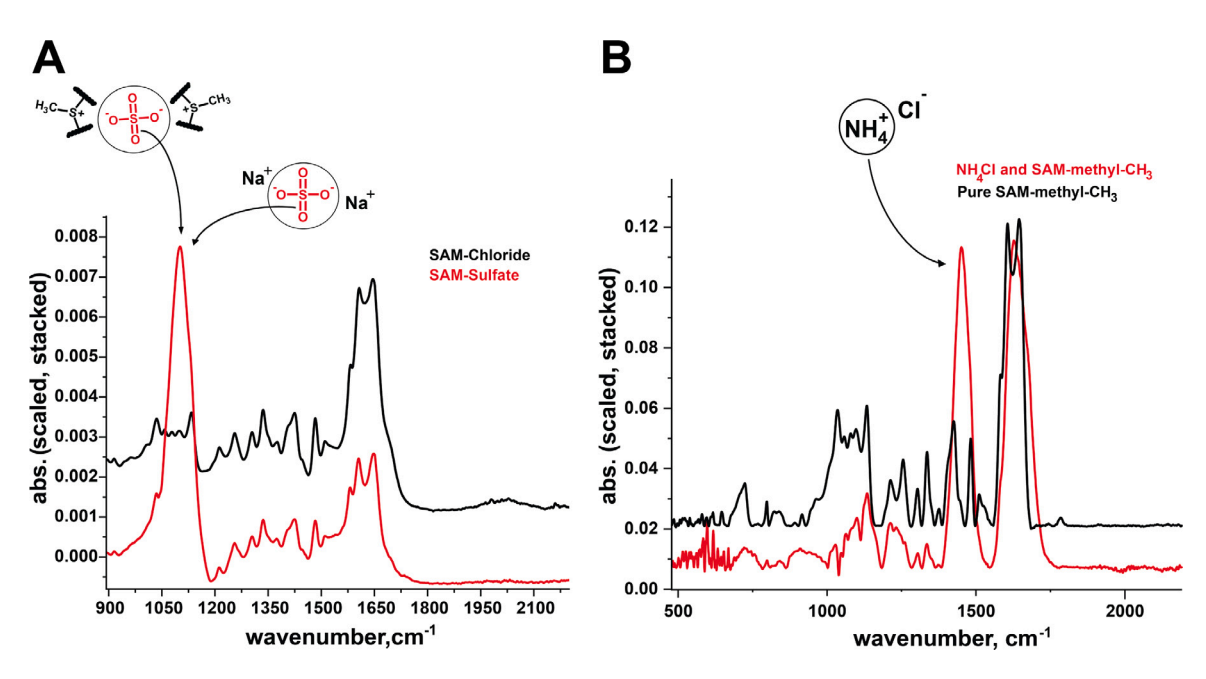


Fig. 7. (A). CD_3 -SAM IR spectrum shows the mean (in bold line) and standard deviation (in the gray-shaded region). In green is the noise line obtained by subtracting two different spectra of the same batch of purified CD_3 -SAM. Perturbation in the C–H stretching region \sim 1100 cm⁻¹ is evidence of isotope incorporation (B) IR spectrum of CH_3 -SAM. The red line is the noise line obtained from the difference between two different spectra of the same batch of purified CH_3 -SAM.

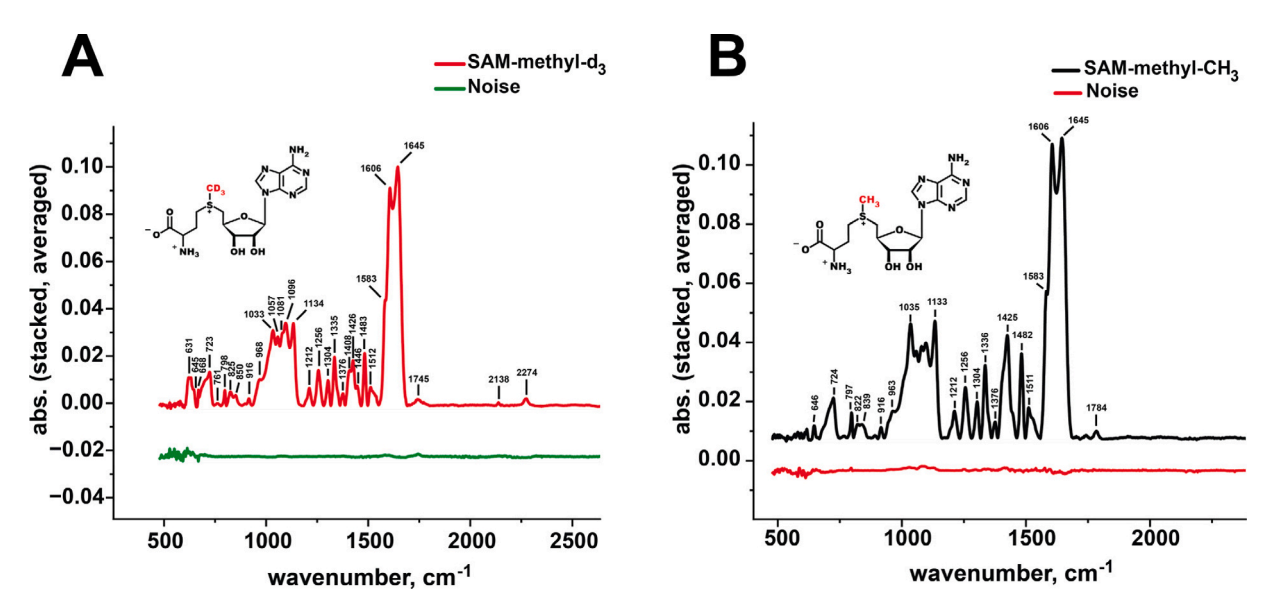


Fig. 8. (A). CD₃-SAM IR spectrum shows the mean (in bold line). In green is the noise line obtained by subtracting two different spectra of the same batch of purified CD₃-SAM. Perturbation in the C–H stretching region 1100 cm-1 is evidence of isotope incorporation (B) IR spectrum of CH₃-SAM. The red line is the noise line obtained from the difference between two different spectra of the same batch of purified CH₃-SAM.

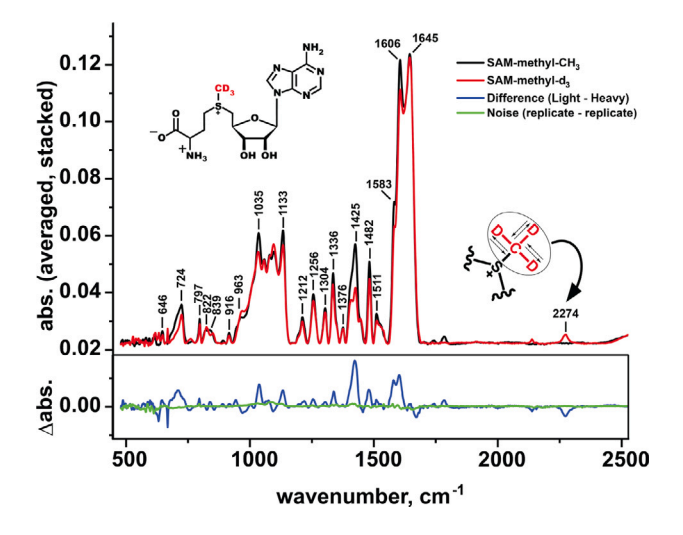


Fig. 9. The spectrum of CD $_3$ -SAM (RED) and CH $_3$ -SAM (BLACK) \sim 100 mM. The noise line (GREEN) was obtained from the natural abundance of CH $_3$ -SAM spectra, and the difference (BLUE) was obtained by subtracting the heavy spectrum from light.

of transition in the linear IR spectrum to specific atomic motions in SAM's molecular structure via isotope labeling. Future work will seek to identify IR signals that will be faithful reporters of SAM's conformation when bound in methyltransferase active sites. These signals can also serve as molecular-scale meters to measure the enthalpies of the noncovalent interactions SAM experiences when in active site environments, which function to accelerate the rates of the myriad of SAM-dependent enzyme-catalyzed reactions [93–95]. In conclusion, our study offers a robust and effective method for obtaining high-quality IR spectra of SAM in solution and lays the foundation for further investigations into the vibrational properties of this important small biomolecule.

CRediT authorship contribution statement

Isaiah Odeyemi: Investigation, Methodology, Writing – original draft, Writing – review & editing, Supervision, Visualization. Teri A. Douglas: Investigation. Nosakhare F. Igie: Investigation. James A.

Hargrove: Investigation, Visualization. Grace Hamilton: Investigation, Visualization. Brianna B. Bradley: Investigation, Visualization. Cathy Thai: Investigation. Brendan Le: Investigation. Maitri Unjia: Investigation. Dylan Wicherts: Investigation, Validation. Zackery Ferneyhough: Investigation, Visualization. Anjali Pillai: Investigation, Visualization. Shailendra Koirala: Investigation, Resources. Laurel M. Hagge: Investigation, Resources. Himanshu Polara: Investigation, Resources. Raymond C. Trievel: Writing – review & editing, Supervision, Resources, Funding acquisition. Robert J. Fick: Conceptualization, Methodology, Writing – original draft, Investigation, Supervision, Writing – review & editing. Allison L. Stelling: Supervision, Writing – review & editing, Funding acquisition, Project administration.

Declaration of competing interest

The authors declare the following financial interests/personal relationships which may be considered as potential competing interests: Allison Stelling reports financial support was provided by National Science Foundation. Allison Stelling reports financial support was provided by Welch Foundation.

Data availability

Data will be made available on request.

Acknowledgments

We acknowledge the National Science Foundation, United States (NSF-CHE-2107902), the Welch Foundation, United States (AT-2079-20210327), and the University of Texas at Dallas, United States startup funds for their invaluable financial support, without which this research project would not have been feasible.

Appendix A. Supplementary data

The detailed method for protein expression and purification, MS, NMR data for SAM.

Supplementary material related to this article can be found online at https://doi.org/10.1016/j.saa.2023.123816.

References

- [1] Shelly C. Lu, S-adenosylmethionine, Int. J. Biochem. Cell Biol. 32 (2000) 391–395
- [2] Matthew R Bennett, Sarah A Shepherd, Victoria A Cronin, Jason Micklefield, Recent advances in methyltransferase biocatalysis, Curr. Opin. Chem. Biol. 37 (2017) 97–106
- [3] Christian Dalhoff, Elmar Weinhold, S-adenosyl-L-methionine and related compounds, in: Modified nucleosides: In biochemistry, biotechnology and medicine, Wiley Online Library, 2008, pp. 223–247.
- [4] Sanja Roje, S-adenosyl-L-methionine: beyond the universal methyl group donor, Phytochemistry 67 (2006) 1686–1698.
- [5] Piotr Z. Kozbial, Arcady R. Mushegian, Natural history of S-adenosylmethioninebinding proteins. BMC Struct. Biol. 5 (2005) 1–26.
- [6] W.A.M. Loenen, S-adenosylmethionine: jack of all trades and master of everything? Biochem. Soc. Trans. 34 (2006) 330–333.
- [7] Robert A. Copeland, Michael E. Solomon, Victoria M. Richon, Protein methyltransferases as a target class for drug discovery, Nat. Rev. Drug Discov. 8 (2009) 724–732.
- [8] Kalpana Ghoshal, Shoumei Bai, DNA methyltransferases as targets for cancer therapy, Drugs Today (Barc) 43 (2007) 395–422.
- [9] Ryuji Hamamoto, Yusuke Nakamura, Dysregulation of protein methyltransferases in human cancer: An emerging target class for anticancer therapy, Cancer Sci. 107 (2016) 377–384.
- [10] Joseph Wanjala Kilwake, Muhammad Jawad Umer, Yangyang Wei, Teame Gereziher Mehari, Richard Odongo Magwanga, Yanchao Xu, Yuqing Hou, Yuhong Wang, Margaret Linyerera Shiraku, Joy Nyangasi Kirungu, Genome-wide characterization of the SAMS gene family in cotton unveils the putative role of GhSAMS2 in enhancing abiotic stress tolerance, Agronomy 13 (2023) 612.
- [11] Margarita E Neganova, Sergey G Klochkov, Yulia R Aleksandrova, Gjumrakch Aliev, Histone Modifications in Epigenetic Regulation of Cancer: Perspectives and Achieved Progress, Vol. 83, Elsevier, 2022, pp. 452–471.
- [12] Agata P Perlinska, Adam Stasiulewicz, Ewa K Nawrocka, Krzysztof Kazimierczuk, Piotr Setny, Joanna I Sulkowska, Restriction of S-adenosylmethionine conformational freedom by knotted protein binding sites, PLoS Comput. Biol. 16 (2020) e1007904.
- [13] M.A. Grillo, Sebastiano Colombatto, S-adenosylmethionine and its products, Amino Acids 34 (2008) 187–193.
- [14] Naeem Shafqat, Joao R C Muniz, Ewa S Pilka, Evangelos Papagrigoriou, Frank von Delft, Udo Oppermann, Wyatt W Yue, Insight into S-adenosylmethionine biosynthesis from the crystal structures of the human methionine adenosyltransferase catalytic and regulatory subunits, Biochem. J. 452 (2013) 27–36.
- [15] Stephen J. Benkovic, Sharon Hammes-Schiffer, A perspective on enzyme catalysis, Science 301 (2003) 1196–1202.
- [16] Arthur I. Cederbaum, Yongke Lu, Defeng Wu, Role of oxidative stress in alcohol-induced liver injury, Arch. Toxicol. 83 (2009) 519–548.
- [17] Ju Chu, Jiangchao Qian, Yingping Zhuang, Siliang Zhang, Yourong Li, Progress in the research of S-adenosyl-L-methionine production, Appl. Microbiol. Biotechnol. 97 (2013) 41–49.
- [18] J. Mann, Epigenetics in Liver Disease: Involvement of Oxidative Stress, Elsevier, 2017, pp. 199–211.
- [19] Giulio L. Cantoni, Biological methylation: selected aspects, Annu. Rev. Biochem. 44 (1975) 435–451.
- [20] Lucy C. Ward, Hannah V. McCue, Andrew J. Carnell, Carboxyl methyltransferases: Natural functions and potential applications in industrial Biotechnology, ChemCatChem 13 (2021) 121–128.
- [21] G.L. Cantoni, The nature of the active methyl donor formed enzymatically from L-methionine and adenosinetriphosphate1, 2, J. Am. Chem. Soc. 74 (1952) 2942–2943.
- [22] James K. Coward, William D. Sweet, Kinetics and mechanism of methyl transfer from sulfonium compounds to various nucleophiles, J. Organ. Chem. 36 (1971) 2337–2346.
- [23] Mark T. Bedford, Stéphane Richard, Arginine methylation: an emerging regulatorof protein function, Mol. Cell 18 (2005) 263–272.
- [24] Mark T. Bedford, Arginine methylation at a glance, J. Cell Sci. 120 (2007) 4243–4246.
- [25] Roméo S. Blanc, Stéphane Richard, Arginine methylation: the coming of age, Mol. cell 65 (2017) 8–24.
- [26] Ernesto Guccione, Stéphane Richard, The regulation, functions and clinical relevance of arginine methylation, Nat. Rev. Mol. Cell Biol. 20 (2019) 642–657.
- [27] Hengyi Jiang, Yanqing Gao, Lei Zhang, Dongrong Chen, Jianhua Gan, Alastair I H Murchie, The identification and characterization of a selected SAM-dependent methyltransferase ribozyme that is present in natural sequences, Nat. Catal. 4 (2021) 872–881.
- [28] Samantha J. Mentch, Jason W. Locasale, One-carbon metabolism and epigenetics: understanding the specificity, Ann. New York Acad. Sci. 1363 (2016) 91–98.
- [29] Jernej Murn, Yang Shi, The winding path of protein methylation research: milestones and new frontiers, Nat. Rev. Mol. Cell Biol. 18 (2017) 517–527.

- [30] Tobias Wagner, Manfred Jung, New lysine methyltransferase drug targets in cancer, Nature Biotechnol. 30 (2012) 622–623.
- [31] Zhouran Wu, Justin Connolly, Kyle K. Biggar, Beyond histones-the expanding roles of protein lysine methylation, FEBS J. 284 (2017) 2732–2744.
- [32] Mareike Albert, Kristian Helin, Histone Methyltransferases in Cancer, Vol. 21, Elsevier, 2010, pp. 209–220.
- [33] Sarah Heerboth, Karolina Lapinska, Nicole Snyder, Meghan Leary, Sarah Rollinson, Sibaji Sarkar, Use of epigenetic drugs in disease: an overview, Genet. Epigenet. 6 (2014) GEG-S12270.
- [34] Dylan Husmann, Or Gozani, Histone lysine methyltransferases in biology and disease, Nat. Struct. Mol. Biol. 26 (2019) 880–889.
- [35] H. Ümit Kaniskan, Kyle D. Konze, Jian Jin, Selective inhibitors of protein methyltransferases, J. Med. Chem. 58 (2015) 1596–1629.
- [36] Keisuke Nimura, Kiyoe Ura, Yasufumi Kaneda, Histone methyltransferases: regulation of transcription and contribution to human disease, J. Mol. Med. 88 (2010) 1213–1220.
- [37] Wahiba Aouadi, Cécilia Eydoux, Bruno Coutard, Baptiste Martin, Françoise Debart, Jean Jacques Vasseur, Jean Marie Contreras, Christophe Morice, Gilles Quérat, Marie-Louise Jung, Toward the identification of viral capmethyltransferase inhibitors by fluorescence screening assay, Antiviral Res. 144 (2017) 330–339.
- [38] Bodo Brueckner, Frank Lyko, DNA methyltransferase inhibitors: old and new drugs for an epigenetic cancer therapy, Trends Pharmacol. Sci. 25 (2004) 551–554.
- [39] David Dilworth, Dalia Barsyte-Lovejoy, Targeting protein methylation: from chemical tools to precision medicines, Cell. Mol. Life Sci. 76 (2019) 2967–2985.
- [40] H. Ümit Kaniskan, Michael L. Martini, Jian Jin, Inhibitors of protein methyltransferases and demethylases, Chem. Rev. 118 (2018) 989–1068.
- [41] Min Wang, Rui-Ming Xu, Paul R. Thompson, Substrate specificity, processivity, and kinetic mechanism of protein arginine methyltransferase 5, Biochemistry 52 (2013) 5430–5440.
- [42] Jing Zhang, Yujun George Zheng, SAM/SAH analogs as versatile tools for SAM-dependent methyltransferases, ACS Chem. Biol. 11 (2016) 583–597.
- [43] Heidi L. Schubert, Robert M. Blumenthal, Xiaodong Cheng, Many paths to methyltransfer: a chronicle of convergence, Trends Biochem. Sci. 28 (2003) 329–335.
- [44] Jessica Bame, Casper Hoeck, Matthew J Carrington, Craig P Butts, Christof M Jäger, Anna K Croft, Improved NOE fitting for flexible molecules based on molecular mechanics data—a case study with S-adenosylmethionine, Phys. Chem. Chem. Phys. 20 (2018) 7523–7531.
- [45] Bin Chen, Xiaobing Zuo, Yun-Xing Wang, T. Kwaku Dayie, Multiple conformations of SAM-II riboswitch detected with SAXS and NMR spectroscopy, Nucleic Acids Res. 40 (2012) 3117–3130.
- [46] Bin Chen, Regan LeBlanc, T. Kwaku Dayie, SAM-II riboswitch samples at least two conformations in solution in the absence of ligand: Implications for recognition, Angew. Chem. 128 (2016) 2774–2777.
- [47] Andrea Haller, Ulrike Rieder, Michaela Aigner, Scott C Blanchard, Ronald Micura, Conformational capture of the SAM-II riboswitch, Nat. Chem. Biol. 7 (2011) 393–400.
- [48] Werner A. Klee, S. Harvey Mudd, The conformation of ribonucleosides in solution. The effect of structure on the orientation of the base, Biochemistry 6 (1967) 988-998
- [49] George D. Markham, Per-Ola Norrby, Charles W. Bock, S-adenosylmethionine conformations in solution and in protein complexes: conformational influences of the sulfonium group, Biochemistry 41 (2002) 7636–7646.
- [50] Gordon G. Hammes, Multiple conformational changes in enzyme catalysis, Biochemistry 41 (2002) 8221–8228.
- [51] Leo C. James, Dan S. Tawfik, Conformational diversity and protein evolution-a 60-year-old hypothesis revisited, Trends Biochem. Sci. 28 (2003) 361–368.
- [52] L. Mario Amzel, Structure-based drug design, Curr. Opin. Biotechnol. 9 (1998) 366–369.
- [53] Amy C. Anderson, The process of structure-based drug design, Chem. Biol. 10 (2003) 787–797.
- [54] Tom L. Blundell, Structure-based drug design, Nature 384 (1996) 23-26.
- [55] Hao Hu, Kun Qian, Meng-Chiao Ho, Y. George Zheng, Small molecule inhibitors of protein arginine methyltransferases, Expert Opin. Investig. Drugs 25 (2016) 335–358.
- [56] Gerhard Klebe, Recent developments in structure-based drug design, J. Mol. Med. 78 (2000) 269–281.
- [57] Renxiao Wang, Ying Gao, Luhua Lai, LigBuilder: a multi-purpose program for structure-based drug design, Mol. Model. Annu. 6 (2000) 498–516.
- [58] Robert E. Benfield, Dario Braga, Brian F.G. Johnson, The question of timescale associated with the determination of molecular structures, Polyhedron 7 (1988) 2549–2552.
- [59] Martin T. Zanni, Robin M. Hochstrasser, Two-dimensional infrared spectroscopy: a promising new method for the time resolution of structures, Curr. Opin. Struct. Biol. 11 (2001) 516–522.
- [60] Kamal Kumar Chaudhary, Nidhi Mishra, A review on molecular docking: novel tool for drug discovery, Databases 3 (2016) 1029.

- [61] Elisabetta Chiarparin, Martin J. Packer, David M. Wilson, Experimental free ligand conformations: a missing link in structure-based drug discovery, 2019, pp. 79–82.
- [62] Pietro Cozzini, Glen E Kellogg, Francesca Spyrakis, Donald J Abraham, Gabriele Costantino, Andrew Emerson, Francesca Fanelli, Holger Gohlke, Leslie A Kuhn, Garrett M Morris, Target flexibility: an emerging consideration in drug discovery and design, J. Med. Chem. 51 (2008) 6237–6255.
- [63] Zengjun Fang, Yu'ning Song, Peng Zhan, Qingzhu Zhang, Xinyong Liu, Conformational restriction: an effective tactic in'follow-on'-based drug discovery, Future Med. Chem. 6 (2014) 885–901.
- [64] G. De La Haba, G.A. Jamieson, S. Harvey Mudd, Henry H. Richards, S-adenosylmethionine: The relation of configuration at the sulfonium center to enzymatic Reactivity1, J. Am. Chem. Soc. 81 (1959) 3975–3980.
- [65] JoséM Mato, Luis Alvarez, Pablo Ortiz, María A Pajares, S-adenosylmethionine synthesis: molecular mechanisms and clinical implications, Pharmacol. Ther. 73 (1997) 265–280.
- [66] Jose R. Matos, Chi-Huey Wong, S-adenosylmethionine: Stability and stabilization, Bioorg. Chem. 15 (1987) 71–80.
- [67] Jeongho Park, Junzhe Tai, Charles A. Roessner, A. Ian Scott, Enzymatic synthesis of S-adenosyl-L-methionine on the preparative scale, Bioorg. Med. Chem. 4 (1996) 2179–2185.
- [68] Hitoshi Kusakabe, Akira Kuninaka, Hiroshi Yoshino, Accumulation of Sadenosylmethionine by molds, Agric. Biol. Chem. 38 (9) (1974) 1669–1672.
- [69] George D. Markham, J. DeParasis, J. Gatmaitan, The sequence of metk, the structural gene for S-adenosylmethionine synthetase in escherichia coli, J. Biol. Chem. 259 (1984) 14505–14507.
- [70] Stanley Goldberg, Mechanical/physical Methods of Cell Distribution and Tissue Homogenization, Springer, 2015, pp. 1–20.
- [71] Haoran Pang, Edward A Lilla, Pan Zhang, Du Zhang, Thomas P Shields, Lincoln G Scott, Weitao Yang, Kenichi Yokoyama, Mechanism of rate acceleration of radical C–C bond formation reaction by a radical SAM GTP 3',8-cyclase, J. Am. Chem. Soc. 142 (2020) 9314–9326, http://dx.doi.org/10.1021/jacs.0c01200.
- [72] Abel Jacobus Bronkhorst, Vida Ungerer, Stefan Holdenrieder, Comparison of methods for the quantification of cell-free DNA isolated from cell culture supernatant, Tumor Biol. 41 (2019) 1010428319866369.
- [73] Wolfgang Becker, Anne Scherer, Christine Faust, David Kornblüh Bauer, Simone Scholtes, Ercole Rao, Joachim Hofmann, Rolf Schauder, Thomas Langer, A fully automated three-step protein purification procedure for up to five samples using the NGC chromatography system, Protein Express. Purif. 153 (2019) 1–6.
- [74] Pacific northwest national laboratory under iarpa contract, 2023, sodium sulphate — webbook.nist.gov. [Accessed 06-11-2023].
- [75] Gautam Das, Nitul Kakati, Seok Hee Lee, Niranjan Karak, Young Soo Yoon, Water soluble sodium sulfate nanorods as a versatile template for the designing of copper sulfide nanotubes, J. Nanosci. Nanotechnol. 14 (6) (2014) 4455–4461.
- [76] Julia Schlesier, Jutta Siegrist, Stefan Gerhardt, Annette Erb, Simone Blaesi, Michael Richter, Oliver Einsle, Jennifer N Andexer, Structural and functional characterisation of the methionine adenosyltransferase from thermococcus kodakarensis, BMC Struct. Biol. 13 (2013) 1–10.

- [77] Malcom W. Chase Jr., NIST-JANAF Thermochemical Tables, Data reported in NIST standard reference database 69, june 2005 release: NIST chemistry WebBook, J. Phys. Chem. Ref. Data Monogr. 9 (1998) 1–1951.
- [78] Johannes Kiefer, Alexander Stärk, Agnita Lynda Kiefer, Heike Glade, Infrared spectroscopic analysis of the inorganic deposits from water in domestic and technical heat exchangers, Energies 11 (2018) 798.
- [79] Jeongho Park, Junzhe Tai, Charles A. Roessner, A. Ian Scott, Overcoming product inhibition of S-adenosyl-L-methionine (SAM) synthetase: Preparation of SAM on the 30 mM scale, Bioorg, Med. Chem. Lett. 5 (1995) 2203–2206.
- [80] Robert A. Alberty, Effect of pH and metal ion concentration on the equilibrium hydrolysis of adenosine triphosphate to adenosine diphosphate, J. Biol. Chem. 243 (1968) 1337–1343.
- [81] Ian F. Tannock, Daniela Rotin, Acid pH in tumors and its potential for therapeutic exploitation, Cancer Res. 49 (1989) 4373–4384.
- [82] Robert A. Alberty, Robert N. Goldberg, Standard thermodynamic formation properties for the adenosine 5'-triphosphate series, Biochemistry 31 (43) (1992) 10610–10615.
- [83] David F. Iwig, Squire J. Booker, Insight into the polar reactivity of the onium chalcogen analogues of S-adenosyl-L-methionine, Biochemistry 43 (2004) 13496–13509.
- [84] Claudia Desiderio, Rosaria A Cavallaro, Antonella De Rossi, Fabrizio D'Anselmi, Andrea Fuso, Sigfrido Scarpa, Evaluation of chemical and diastereoisomeric stability of S-adenosylmethionine in aqueous solution by capillary electrophoresis, J. Pharm. Biomed. Anal. 38 (2005) 449–456.
- [85] Timm Lankau, Tzu Nung Kuo, Chin Hui Yu, Computational study of the degradation of S-adenosyl methionine in water, J. Phys. Chem. A 121 (2017) 505–514.
- [86] Mark L. Stolowitz, M.J. Minch, S-adenosyl-L-methionine and S-adenosyl-L-homocysteine, an NMR study, J. Am. Chem. Soc. 103 (1981) 6015–6019.
- [87] Francisco C. Nart, Teresa Iwasita, Martin Weber, Sulfate adsorption on well-defined Pt (100) electrodes, Electrochim. Acta 39 (1994) 2093–2096.
- [88] Inc. Coblentz Society, Sodium sulfate, 1970.
- [89] Chih-Kai Lin, Jer-Lai Kuo, Anharmonic IR spectra of solvated ammonium and aminium ions: resemblance between water and bisulfate solvations, Phys. Chem. Chem. Phys. 24 (2022) 20318–20325.
- [90] Jean-Joseph Max, Camille Chapados, Aqueous ammonia and ammonium chloride hydrates: Principal infrared spectra, J. Mol. Struct. 1046 (2013) 124–135.
- [91] A. Lee Smith, The coblentz society desk book of infrared spectra, 2, 1982.
- [92] Xiao-Nan Wei, Min-Jie Cao, Jian Li, Huan Li, Yi Song, Cui-Hong Du, Synthesis of S-adenosyl-L-methionine in escherichia coli, Biotechnol. Bioprocess Eng. 19 (2014) 958–964.
- [93] Catherine Berthomieu, Rainer Hienerwadel, Fourier transform infrared (FTIR) spectroscopy, Photosynth. Res. 101 (2009) 157–170.
- [94] Carsten Kötting, Klaus Gerwert, Proteins in action monitored by time-resolved fTIR spectroscopy, ChemPhysChem 6 (2005) 881–888.
- [95] Lily M. Ng, Reiko Simmons, Infrared spectroscopy, Anal. Chem. 71 (1999) 343–350.